Tracking the subsurface path of dislocations in GaN using scanning tunneling microscopy

P. H. Weidlich,[1] M. Schnedler,[1] V. Portz,[1] H. Eisele,[2] U. Strauß,[3] R. E. Dunin-Borkowski,[1] and Ph. Ebert[1,a)]
[1]*Peter Grünberg Institut, Forschungszentrum Jülich GmbH, 52425 Jülich, Germany*
[2]*Institut für Festkörperphysik, Technische Universität Berlin, Hardenbergstr. 36, 10623 Berlin, Germany*
[3]*OSRAM Opto-Semiconductors GmbH, Leibnizstr. 4, 93055 Regensburg, Germany*

(Received 7 May 2015; accepted 3 July 2015; published online 15 July 2015)

A methodology for the determination of the subsurface line direction of dislocations using scanning tunneling microscopy (STM) images is presented. The depth of the dislocation core is derived from an analysis of the displacement field measured by STM. The methodology is illustrated for dislocations at GaN($10\bar{1}0$) cleavage surfaces. It is found that the dislocation line bends toward the surface, changing from predominantly edge-type to more screw-type character, when approaching the intersection point. Simultaneously, the total displacement detectable at the surface increases due to a preferred relaxation towards the surface. © *2015 AIP Publishing LLC*.
[http://dx.doi.org/10.1063/1.4926789]

I. INTRODUCTION

Dislocations commonly affect the electronic properties of semiconductors and have the potential to critically degrade electronic and optoelectronic semiconductor devices.[1,2] The influence of dislocations primarily arises from the introduction of localized defect states, which may give rise to electrical charges and/or conduction channels along the dislocation line. For most semiconductors, in particular for GaN, the existence of such defect states and/or localized charges at dislocation cores has been predicted theoretically.[3–9] Experimentally, electrical charges along dislocation lines were identified, too, mostly using microscopy-based methods.[10–17] Despite these efforts, a comprehensive understanding of the electronic properties of dislocations is a tremendous task still. This is due to the fact that the electronically relevant density of defect states and electrical charges depend sensitively on the exact atomic structure of the dislocation core, which itself is governed by many parameters. The most obvious parameters are the impurity and doping concentration of the material, the strain field in the device structures, as well as the type of dislocations, i.e., its Burgers vector and the orientation of the dislocation line.

The line direction is particularly relevant for group III-nitride semiconductors: Due to the lack of affordable and sufficiently large real bulk substrates, group III-nitride layers are grown mostly on non lattice and thermally matched substrates or on pseudo substrates. This induces rather large dislocation concentrations far beyond those characteristic for the classical III-V semiconductors.[18] Therefore, the need to reduce the dislocation concentrations has led to growth schemes, where the dislocation lines are bent off the growth direction.[19–26] Hence, most dislocations are not present in their original line direction and may thus change their electronic properties. Therefore, it is particularly relevant to be able to identify the line direction of the dislocation cores.

a)Electronic mail: p.ebert@fz-juelich.de

It is generally known that the orientation of the line direction of a dislocation and its Burgers vector can be readily determined by transmission electron microscopy (TEM). However, surface sensitive techniques are frequently used to map the dislocation concentration, e.g., by counting pit densities in scanning electron or atomic force microscopy images,[27,28] or by directly imaging and counting the dislocation cores intersecting the surface, e.g., by scanning tunneling microscopy (STM).[29,30] STM has also been used to determine the atomic[31–33] and electronic[15] structure of dislocation cores at their intersection point with the surface. Therefore, it is desirable to develop a simple methodology to determine the subsurface path and hence the line direction of dislocations intersecting surfaces using surface-sensitive microscopy techniques. Thus far, the line direction was either *a priori* known as in case of buried misfit dislocations at hetero interfaces.[34–36] For in the first place unknown orientations of dislocations, the *projected* line direction was derived from STM images of the displacement field,[17] or molecular dynamics simulations were used to calculate the subsurface dislocation structure and correlate this with the dislocation-induced step height at the surface.[37,38] However, the latter approach is rather complex and time-consuming, inhibiting its use for large numbers of dislocations, and the former approach does not contain the subsurface depth information.

In this paper, we illustrate the determination of the depth of a subsurface dislocation core using the displacement field at the surface measured by STM. The spatial variation of the depth along the dislocation line allows to follow its subsurface path and hence the line direction of the dislocation core. On basis of the depth information near the intersection point of the dislocation with the surface, we determine the intersection angle.

II. EXPERIMENT

The aim of the experiments is to probe the displacement fields surrounding dislocations intersecting a surface. We

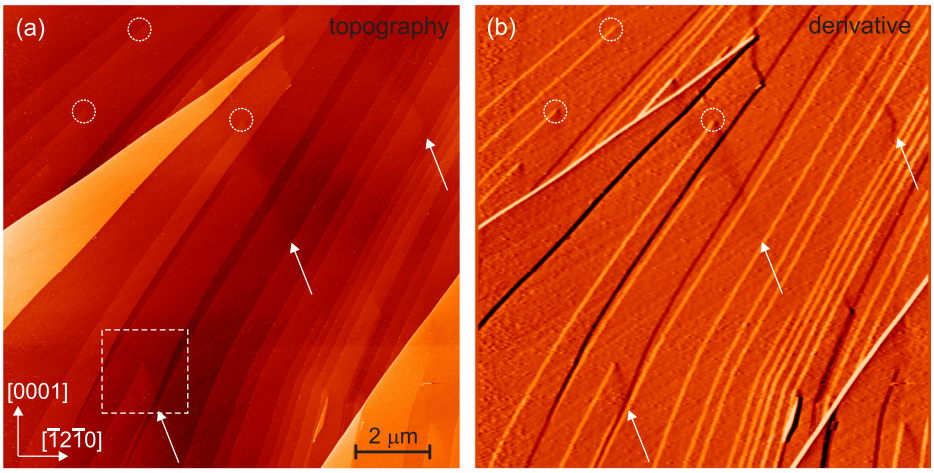

FIG. 1. (a) Constant-current STM image and (b) directional derivative of the STM image along the [$\bar{1}2\bar{1}0$] direction of the GaN(10$\bar{1}$0) cleavage surface measured at a voltage of +4 V and a tunnel current of 50 pA. In this cross-sectional view, the growth direction of the epitaxial GaN layers is toward the top ([0001] direction). The surface exhibits terraces separated by steps. The total topographic height difference is 18 ML (~5 nm) in the area shown. Some of the steps terminate suddenly at dislocations intersecting the cleavage surface. The strain fields introduced by the dislocations induce distortions of the surface plane (highlighted in the derivative image). In some cases, these distortions extend far away from the intersection point (arrows), indicating the presence of shallow subsurface dislocation cores. The area indicated by the dashed rectangular in (a) is enlarged in Fig. 2.

chose GaN epitaxial layers since this material typically exhibits rather large dislocation densities,[18] which enables us to find sufficient numbers of dislocations intersecting the limited surface areas scanned by STM.[17,30]

Thus, the experiments are performed on non-polar GaN(10$\bar{1}$0) surfaces obtained by cleaving epitaxially grown *n*-type GaN(0001) layers with carrier concentrations of a few 10^{18} cm^{-3}. In order to improve the cleavage, rectangular-shaped samples (long axis in $\langle 10\bar{1}0\rangle$ direction) were thinned. The bottom half is electrically contacted by sputtered Au contacts and mounted into the sample holder. Cleaving off the upper, non contacted free standing part of the samples in ultrahigh vacuum (1×10^{-8} Pa) yields contamination free and clean GaN(10$\bar{1}$0) surfaces, which represent a cross-sectional view through the epitaxial layers perpendicular to the [0001] growth direction.

After cleavage, the samples are transferred into the STM chamber without breaking the vacuum and investigated by STM in the constant-current mode. This mode records a superposition of topography and electronic effects. The main contrast is, however, topographic, since electronic effects are negligible: (i) The local atomic structure within a 1×1 unit cell, visible in high resolution STM images,[39–42] is averaged at our magnifications. (ii) The screened Coulomb potential around localized charges at the surface induce voltage dependent depressions or elevations,[43–45] which typically vanish at the used voltages of 4 V.[46–48] Potential fluctuations with spatial dimensions of 30–40 nm due to inhomogeneities in the dopant distribution[49–51] also weaken at the high voltages used. They are still slightly visible in the STM images, but give rise to local height variation of only ~0.03 nm, i.e., $\frac{1}{10}$ ML appearing as noise. Since we analyze the long range effects over several 100 nm, this does not affect the results.

III. EXPERIMENTAL RESULTS

Figure 1(a) shows a constant-current STM image of the GaN(10$\bar{1}$0) cleavage surface. In this cross-sectional view of the cleaved GaN epitaxial layer, the [0001] growth direction is oriented to the top side. The surface morphology is governed by large terraces separated by steps of various heights. Most steps are one monolayer high steps (step height of 2.76 Å). These steps frequently terminate suddenly (see examples marked by dashed circles). At such termination points of steps, a dislocation intersects with the surface.[17,31,33,52–54] We observed an average dislocation density of 1.5×10^7 cm^{-2}, which exhibits, however, significant spatial fluctuations.[30] The actual dislocation density is about 50% larger, since without atomic resolution we cannot observe dislocations with in plane Burgers vectors.[30]

The contrast of the STM image in Fig. 1(a) indicates that the surface surrounding the intersection points of dislocations is not planar, but rather deformed vertically. This suggests that most dislocations introduce a significant displacement field. To highlight the local deformation of the surface plane due to strain fields, Fig. 1(b) shows the directional derivative of the STM image along the [$\bar{1}2\bar{1}0$] direction. The steps appear either as bright or dark lines. At the termination points of the steps, one can recognize frequently a directionally oriented displacement field (mostly showing up as darker zone in this derivative STM image due to the predominant Burgers vectors present in this area). This non symmetric strain field arises from the inclined penetration of the dislocation line into the surface, relaxing the surface plane locally above the subsurface dislocation core.[17] The directionally oriented strain field is usually only detectable rather close to the intersection point of the dislocation with the surface, since the dislocation core is quickly too deep below the surface to be detectable. In some cases, however, the surface is also deformed at very large distances (up to 4 μm) from the intersection point as outlined by the two lower arrows in Fig. 1. The upper-rightmost arrow marks even a strain field induced by a subsurface dislocation, which appears to never reach and penetrate the surface.

In the following, we concentrate on the dislocation marked by the dashed rectangle in Fig. 1(a). Figure 2(a)

shows an enlarged view of this dislocation. The intersection point is at the center of the dashed circle at the position where the step terminates. Most of the deformation of the surface is spatially localized in a rather narrow region extending from the intersection point toward the lower right corner of the STM image (defined as $-x$ direction). Figure 2(b) shows circular height profiles of the surface topography surrounding the intersection point of the dislocation at the surface. The height change is visibly not distributed evenly over the whole range of angles ω, as expected for dislocations with a line direction and Burgers vector perpendicular to the surface (i.e., screw dislocations).[55,56] Instead, most of the height change occurs in a narrow angular range close to $\omega = 180°$. This shape of the displacement field indicates that the dislocation line is penetrating the surface toward the lower right corner with a shallow angle. The highest displacement changes in the profiles (also visible as dark line in the derivative of the height in Fig. 1(b)) traces the projection of the subsurface dislocation line onto the surface, which is defined as $-x$ direction in the following.

The strain field can be visualized further by analyzing height profiles along the y direction on the lower right side of intersection point at the positions labeled as (a)–(e) in Fig. 2(a). Figure 3 illustrates these five selected profiles using the same colors as the dashed lines marking their positions in Fig. 2(a). Each height profile consists of the average of 8 neighboring height profiles (corresponding to a spatial average over approximately 50 nm along x direction). The line profiles exhibit clearly a displacement of the plane from the left to the right side. For line profiles close to the intersection

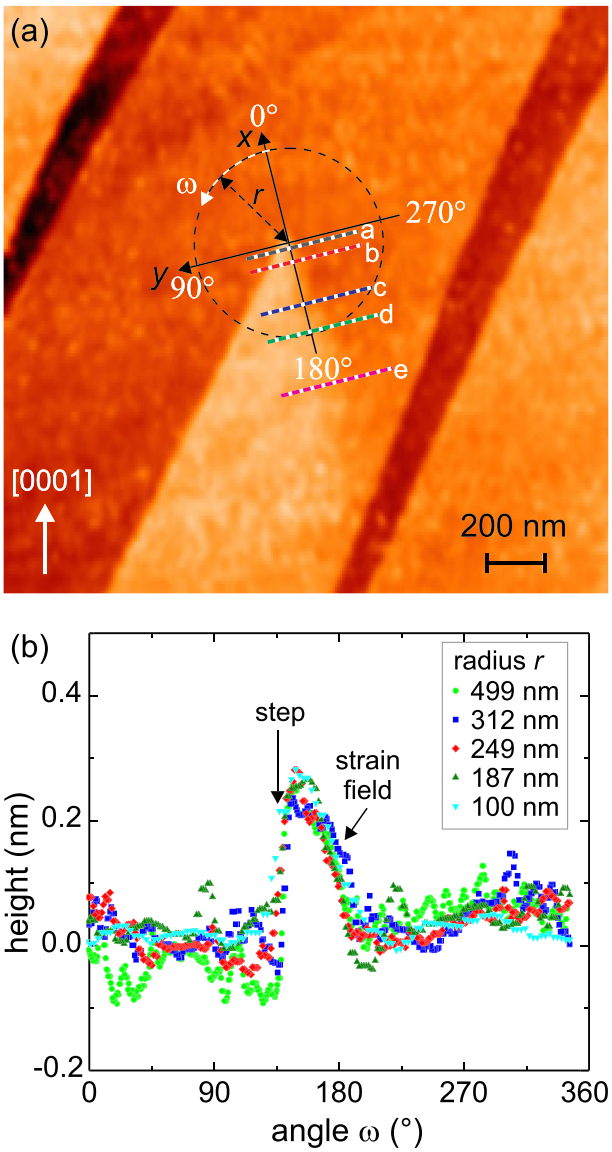

FIG. 2. (a) Enlarged constant current STM image of the dislocation in the dashed rectangular in Fig. 1(a). The intersection point of the dislocation and the surface is at the center of the dashed circle where the one monolayer high surface step terminates. The surface plane is deformed toward the lower right ($-x$) direction due to the displacement field induced by the subsurface dislocation core. Hence, the surface projected line direction of the dislocation follows the $-x$ direction starting at the origin of the chosen coordinate system. The topographic height difference is 2 ML. (b) Circular height profiled around the dislocation intersection point measured at different radii around the dislocation is shown in (a). The angle ω is set to zero in $+x$ direction. The height changes only in a very small angular region around $\omega = 180°$. The step induces a height change of 1 ML (=2.76 Å) at $\omega \approx 140°$.

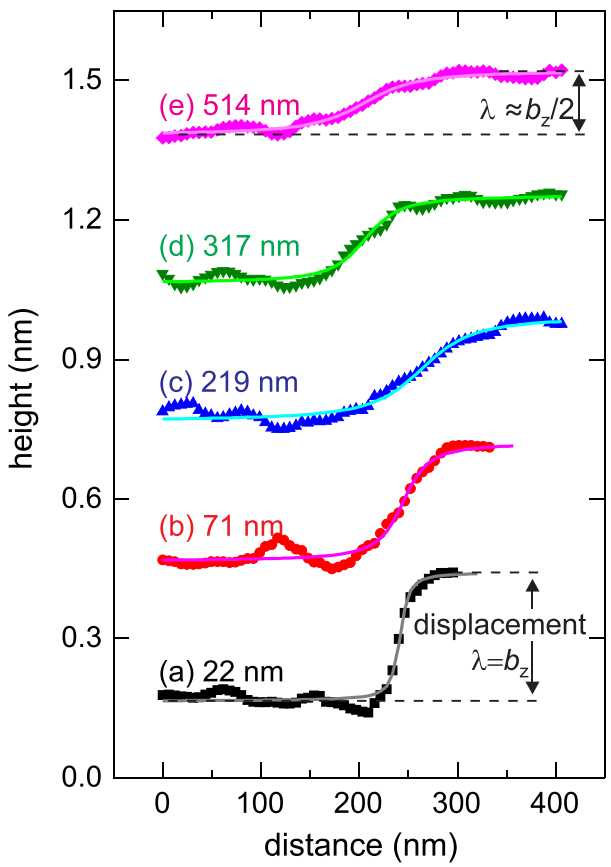

FIG. 3. Selection of analyzed height profiles measured parallel to the y axis (symbols). The spatial position and length of the height profiles are indicated by the colored dotted lines in Fig. 2(a). Each height profile consists of the average of 8 neighboring height profiles corresponding to a spatial width of approximately 50 nm. The solid lines represent the fits of Eq. (1) to the experimental data. The height profiles have been offset by 0.3 nm for clarity. The distance of the selected profiles to the intersection point of the dislocation is given at their respective left end. The total out-of-plane displacement of the surface plane on the left and right side is labelled as λ. Close to the intersection point, the out-of-plane displacement equals the vertical component of the Burgers vector b_z. Far away the out-of-plane displacement decays to $\approx \frac{1}{2} b_z$.

point of the dislocation [Fig. 3 profile (a), 22 nm distance], the total out-of-plane displacement is 1 monolayer, becoming smaller with increasing distance [profile (e), 514 nm distance].

IV. DETERMINATION OF THE DEPTH OF THE DISLOCATION CORE

In order to determine the depth of the dislocation core, we have to address the Burgers vector of the dislocation first. GaN may contain different types of dislocations with a, c, or $(a+c)$-type Burgers vectors. Pure c-type dislocations with a Burgers vector in c direction do not induce a step on a nonpolar surface plane and hence cannot be observed in Fig. 1 without atomic resolution. The dislocations observed here were found to have all an *out-of-plane* component (vertical to the surface) of the Burgers vector of one monolayer step height (i.e., $\frac{a}{2}[10\bar{1}0]$). The step also points to an *in-plane* component of the Burgers vector (parallel to the atomic rows within the surface plane), because two neighboring $(11\bar{2}0)$ planes in the wurtzite structure are offset by $\frac{a}{6}[11\bar{2}0]$. This morphology is consistent with a perfect dislocation with a Burgers vector of $\frac{a}{3}\langle 11\bar{2}0\rangle$, tilted 30° with respect to the surface normal.[17] This type of dislocation is the one primarily observed at the cleavage surfaces.[17] And the only possible one without any component of the Burgers vector along the [0001] direction in wurtzite crystals.[57]

For the further analysis, we assume that the in-plane and out-of-plane displacement fields can be treated separately. This assumption is valid for isotropic media and sufficiently far away from the dislocation core, where the distortions can be treated elastically and linearly.[58] Since at our resolution we only detect the out-of-plane distortions perpendicular to the surface plane in z-direction, we focus in the following on the component of the Burgers vector perpendicular to the surface. The resulting displacements can be described as those of a subsurface edge dislocation with line direction along the x direction and a Burgers vector perpendicular to the surface plane (z direction). The insertion of an atomic plane at the core of the edge dislocation (at the depth position z) locally disrupts the symmetry of the crystal lattice and hence exerts strain onto the crystal.[59] The local displacements were derived analytically on basis of the Airy stress function.[55,60–63] The out-of-plane displacement d_z in z direction, which is relevant for the displacements probed in the STM images, is given by the following equation:[56,61]

$$d_z = \frac{\lambda}{2\pi}\cdot\left(\arctan\left(\frac{y}{z}\right)+\frac{1}{2(1-\nu)}\cdot\frac{z\cdot y}{z^2+y^2}\right), \qquad (1)$$

with ν being the Poisson's ratio. λ is the total amount the material is displaced $(\lambda = d_z(y=\infty) - d_z(y=-\infty))$ by the z component of the Burgers vector b_z. This equation can be used to calculate the local displacements induced by an edge dislocation in an infinitely extended bulk crystal. In this case, the total displacement λ equals $\pm\frac{1}{2}b_z$ for the half spaces $z>0$ and $z<0$, respectively, since—due to symmetry reasons—one can assume an equal relaxation of the strain in $+z$ and $-z$ directions.

For a dislocation close to a surface, the assumption of equal relaxation of the strain field in $+z$ and $-z$ directions is, however, not necessarily applicable. Directly at the intersection point, the displacement introduced by the Burgers vector will fully relax only to the surface side. This is corroborated by the observed step heights, which correspond directly to the complete out-of-plane component of the Burgers vector. With increasing depth, the strain field is increasingly symmetrically distributed toward the $+z$ and $-z$ directions, changing the total displacement observed at the surface from b_z to $\frac{1}{2}b_z$. Since we do not know from which depth on a symmetrical relaxation occurs, the displacement observed at the surface is one relevant physical parameter to be determined.

In the absence of a more elaborate displacement model, we assume that the functional form of the displacement at the surface can be approximated by Eq. (1). Since the dislocation core may have a varying depth along the dislocation line, we fit this equation to the height profiles measured in STM images at different x positions along the surface projected dislocation line, using the total displacement λ and the depth z as fitting parameters.

The solid lines in Fig. 3 show the best fits of Eq. (1) to the selected height profiles. The fits reproduce well the slope and the width over which the displacement changes as well as the total displacements. Figure 3 shows that the width increases with increasing distance from the intersection point. This translates qualitatively into an increasing depth of the dislocation core. Figure 4 illustrates the quantitative depth values determined for different distances to the intersection point from fits such as those selected in Fig. 3. The

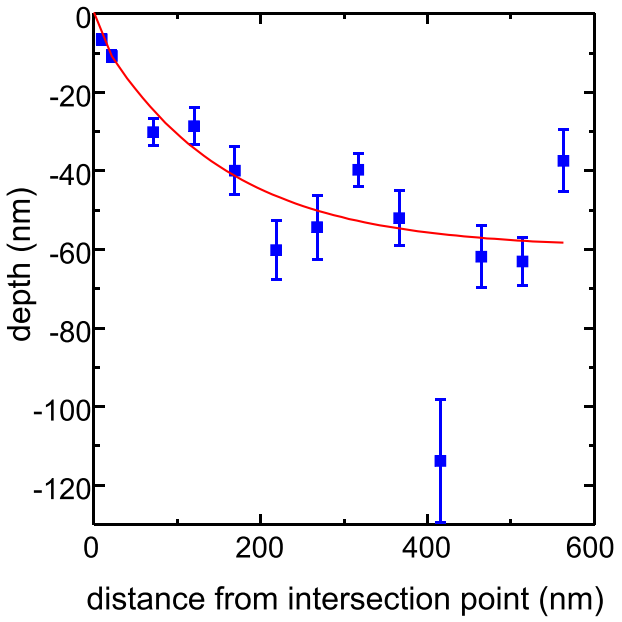

FIG. 4. Depth of the dislocation core below the surface as a function of the distance from the intersection point of the dislocation on the surface. The depth is obtained from the fits of Eq. (1) to the height profiles in Figure 3. The error bar on each depth mainly depends on the noise of the image as well as on the number of averaged line profiles. In order to highlight the approximate subsurface path of the dislocation core, an exponential decay $(z(x) = a\cdot e^{-|x|/b} + z_0)$ was fitted to the depth values (red solid line). The initial penetration angle close to the intersection point is about 20°, decreasing with increasing separation.

error of each depth value is primarily determined by the noise in the STM image and the number of averaged line profiles entering each height profile. Furthermore, the values are sensitive to an additional slope induced by the sample-scanner tube misalignment and the non linearity of the scanner tube. Therefore, we corrected all STM images for the scanning distortions using the technique outlined in Ref. 64 and removed any additional slope assuming that the large terraces are atomically flat at sufficiently large distances from dislocation cores. Such determined depth values versus distance trace the subsurface position of the dislocation line in $-x$ direction.

The depth of the dislocation line in Fig. 4 increases roughly linearly up to a distance to the intersection point of 200 nm. Beyond 400 nm distance, the depth reaches a constant value. Note, the very large depth value with very large error bar (and the corresponding large displacement value, see Fig. 5) at about 420 nm distance is due to a very noisy height profile at this distance. It should be considered with care only. The fit to the data, with weighting using the error bars, (solid line in Fig. 4) shows that this depth profile can be described tentatively by an exponential decay $z(x) = a \cdot e^{-|x|/b} + z_0$ with $a = 56.3 \pm 4.5$ nm, $b = 151.1 \pm 36$ nm, and $z_0 = -59.7 \pm 5$ nm. This fit illustrates that the penetration angle decreases from $20.4 \pm 4.5^\circ$ close to the intersection point down to $\approx 1^\circ$ at 400–500 nm distance. Hence, the dislocation line is almost parallel to the surface plane at large distances and bends toward the surface plane when approaching the intersection point. This suggests a predominantly edge type character of the dislocation in the bulk, becoming more screw like at the surface. This general behavior is also found for dislocations initially oriented along the [0001] growth direction if inclined facets appear during growth of GaN epitaxial layers. The dislocations then bend toward the inclined facet,[19–21,23,25,26,65] in order to minimize the line energy by shortening its length. Note, the dislocations in the cleaved samples likely do not reach their equilibrium line directions after cleavage at room temperature. The line direction is predominantly a frozen-in configuration, despite it is known, that the STM tip can excite the slip of dislocations.[33]

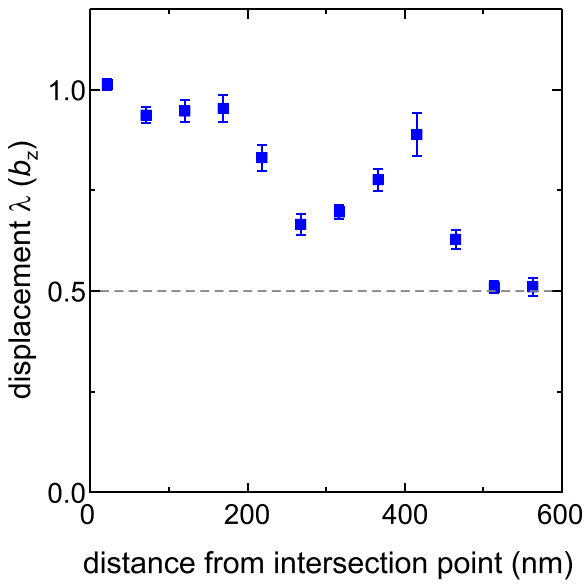

FIG. 5. Total displacement λ in units of the vertical component of the Burgers vector b_z as a function of the distance from the intersection point.

Figure 5 illustrates the total displacement λ in units of the out-of-plane component of the Burgers vector b_z versus the distance from the intersection point. λ is obtained from the fits of Eq. (1) to the height profiles. Close to the intersection point, i.e., where the dislocation is directly at the surface, the total displacement equals $b_z = 2.76$ Å. With increasing distance from the intersection point—and hence increasing depth—λ decreases to $\frac{1}{2} b_z$. This trend can be understood as the effect the surface has on the relaxation of strain and the distribution of displacements. Deep in the bulk, the relaxation is symmetrical and the displacement is divided equally in both half spaces. For a subsurface dislocation close to the surface, the limited number of atomic layers to the surface side effectively weakens the material, favoring a relaxation of the atoms toward the surface side. The data suggest that for GaN $(10\bar{1}0)$ surfaces this surface relaxation effect is relevant up to approximately 60 nm depth.

V. SUMMARY

In summary, a methodology is presented to determine the depth of subsurface dislocations on basis of their displacement field at the surface measured by scanning tunneling microscopy. This allows to track the subsurface path of dislocations. The methodology is illustrated for dislocations intersecting GaN $(10\bar{1}0)$ surfaces. The line of the particular dislocation discussed is found to bend toward the surface when approaching the intersection point with the surface. The displacement fields visible at the surface suggest that this bending is a typical behavior of subsurface dislocations. Finally, the strain field of subsurface dislocations in GaN $(10\bar{1}0)$ does not relax symmetrically, but rather favors the relaxation of atoms toward the surface side up to a depth of about 60 nm. This suggests that the presence of the surface weakens the near surface material.

ACKNOWLEDGMENTS

The authors thank K. H. Graf for technical support and the Deutsche Forschungsgemeinschaft for financial support under Grant Nos. Eb197/5-1 and Ei788/2-1.

[1]H. Alexander, *Dislocations in Solids* (North Holland, Amsterdam, 1986), p. 113.
[2]H. Morkoç, *Nitride Semiconductor Devices: Fundamentals and Applications* (John Wiley & Sons, 2013).
[3]J. Elsner, R. Jones, P. K. Sitch, V. D. Porezag, M. Elstner, T. Frauenheim, M. I. Heggie, S. Öberg, and P. R. Briddon, Phys. Rev. Lett. **79**, 3672 (1997).
[4]Y. Xin, S. J. Pennycook, N. D. Browning, P. D. Nellist, S. Sivananthan, F. Omnes, B. Beaumont, J. P. Faurie, and P. Gibart, Appl. Phys. Lett. **72**, 2680 (1998).
[5]A. F. Wright and U. Grossner, Appl. Phys. Lett. **73**, 2751 (1998).
[6]A. T. Blumenau, J. Elsner, R. Jones, M. I. Heggie, S. Öberg, T. Frauenheim, and P. R. Briddon, J. Phys.: Condens. Matter **12**, 10223 (2000).
[7]J. E. Northrup, Phys. Rev. B **66**, 045204 (2002).
[8]L. Lymperakis, J. Neugebauer, M. Albrecht, T. Remmele, and H. P. Strunk, Phys. Rev. Lett. **93**, 196401 (2004).
[9]I. Belabbas, J. Chen, P. Komninou, and G. Nouet, Comput. Mater. Sci. **79**, 118 (2013).

[10]P. J. Hansen, Y. E. Strausser, A. N. Erickson, E. J. Tarsa, P. Kozodoy, E. G. Brazel, J. P. Ibbetson, U. Mishra, V. Narayanamurti, S. P. DenBaars, and J. S. Speck, Appl. Phys. Lett. **72**, 2247 (1998).
[11]D. Cherns and C. G. Jiao, Phys. Rev. Lett. **87**, 205504 (2001).
[12]G. Koley and M. G. Spencer, Appl. Phys. Lett. **78**, 2873 (2001).
[13]J. Cai and F. Ponce, Phys. Status Solidi A **192**, 407 (2002).
[14]J. W. P. Hsu, H. M. Ng, A. M. Sergent, and S. N. G. Chu, Appl. Phys. Lett. **81**, 3579 (2002).
[15]Ph. Ebert, C. Domke, and K. Urban, Appl. Phys. Lett. **78**, 480 (2001).
[16]A. Hinoki, J. Kikawa, T. Yamada, T. Tsuchiya, S. Kamiya, M. Kurouchi, K. Kosaka, T. Araki, A. Suzuki, and Y. Nanishi, Appl. Phys. Express **1**, 011103 (2008).
[17]Ph. Ebert, L. Ivanova, S. Borisova, H. Eisele, A. Laubsch, and M. Dähne, Appl. Phys. Lett. **94**, 062104 (2009).
[18]P. Gibart, Rep. Prog. Phys. **67**, 667 (2004).
[19]P. Vennéguès, B. Beaumont, V. Bousquet, M. Vaille, and P. Gibart, J. Appl. Phys. **87**, 4175 (2000).
[20]K. Hiramatsu, K. Nishiyama, M. Onishi, H. Mizutani, M. Narukawa, A. Motogaito, H. Miyake, Y. Iyechika, and T. Maeda, J. Cryst. Growth **221**, 316 (2000).
[21]A. Sakai, H. Sunakawa, and A. Usui, Appl. Phys. Lett. **73**, 481 (1998).
[22]O. Contreras, F. Ponce, J. Christen, A. Dadgar, and A. Krost, Appl. Phys. Lett. **81**, 4712 (2002).
[23]A. E. Romanov, P. Fini, and J. S. Speck, J. Appl. Phys. **93**, 106 (2003).
[24]S. Gradeçak, P. Stadelmann, V. Wagner, and M. Ilegems, Appl. Phys. Lett. **85**, 4648 (2004).
[25]R. Datta and C. J. Humphreys, Phys. Status Solidi C **3**, 1750 (2006).
[26]J. K. Farrer and C. B. Carter, J. Mater. Sci. **41**, 779 (2006).
[27]K. Shiojima, J. Vac. Sci. Technol., B **18**, 37 (2000).
[28]L. Lu, Z. Y. Gao, B. Shen, F. J. Xu, S. Huang, Z. L. Miao, Y. Hao, Z. J. Yang, G. Y. Zhang, X. P. Zhang, J. Xu, and D. P. Yu, J. Appl. Phys. **104**, 123525 (2008).
[29]A. R. Smith, V. Ramachandran, R. M. Feenstra, D. W. Greve, M.-S. Shin, M. Skowronski, J. Neugebauer, and J. E. Northrup, J. Vac. Sci. Technol., A **16**, 1641 (1998).
[30]P. H. Weidlich, M. Schnedler, H. Eisele, R. Dunin-Borkowski, and Ph. Ebert, Appl. Phys. Lett. **103**, 142105 (2013).
[31]G. Cox, D. Szynka, U. Poppe, K. H. Graf, K. Urban, C. Kisielowski-Kemmerich, J. Krüger, and H. Alexander, Phys. Rev. Lett. **64**, 2402 (1990).
[32]G. Cox, D. Szynka, U. Poppe, K. H. Graf, K. Urban, C. Kisielowski-Kemmerich, J. Krüger, and H. Alexander, Phys. Rev. Lett. **65**, 387 (1990).
[33]G. Cox, Ph. Ebert, U. Poppe, M. Simon, and K. Urban, Ultramicroscopy **42–44**, 776 (1992).
[34]G. Springholz, G. Bauer, and V. Holy, Phys. Rev. B **54**, 4500 (1996).
[35]G. Springholz, Appl. Surf. Sci. **112**, 12 (1997).
[36]J. G. Belk, D. W. Pashley, B. A. Joyce, and T. S. Jones, Phys. Rev. B **58**, 16194 (1998).
[37]J. Christiansen, K. Morgenstern, J. Schiøtz, K. W. Jacobsen, K.-F. Braun, K.-H. Rieder, E. Lægsgaard, and F. Besenbacher, Phys. Rev. Lett. **88**, 206106 (2002).
[38]J. Engbæk, J. Schiøtz, B. Dahl-Madsen, and S. Horch, Phys. Rev. B **74**, 195434 (2006).
[39]L. Ivanova, S. Borisova, H. Eisele, M. Dähne, A. Laubsch, and Ph. Ebert, Appl. Phys. Lett. **93**, 192110 (2008).
[40]M. Bertelli, P. Löptien, M. Wenderoth, A. Rizzi, R. G. Ulbrich, M. C. Righi, A. Ferretti, L. Martin-Samos, C. M. Bertoni, and A. Catellani, Phys. Rev. B **80**, 115324 (2009).
[41]B. Siemens, C. Domke, Ph. Ebert, and K. Urban, Phys. Rev. B **56**, 12321 (1997).
[42]L. Lymperakis, P. H. Weidlich, H. Eisele, M. Schnedler, J.-P. Nys, B. Grandidier, D. Stievenard, R. E. Dunin-Borkowski, J. Neugebauer, and Ph. Ebert, Appl. Phys. Lett. **103**, 152101 (2013).
[43]J. A. Stroscio, R. M. Feenstra, and A. P. Fein, Phys. Rev. Lett. **58**, 1668 (1987).
[44]Ph. Ebert, Surf. Sci. Rep. **33**, 121 (1999).
[45]Ph. Ebert, Curr. Opinion Solid State Mater. Sci. **5**, 211 (2001).
[46]Ph. Ebert and K. Urban, Ultramicroscopy **49**, 344 (1993).
[47]Ph. Ebert, M. Heinrich, M. Simon, K. Urban, and M. G. Lagally, Phys. Rev. B **51**, 9696 (1995).
[48]Ph. Ebert, M. Heinrich, M. Simon, C. Domke, K. Urban, C. Shih, M. Webb, and M. Lagally, Phys. Rev. B **53**, 4580 (1996).
[49]N. D. Jäger, K. Urban, E. R. Weber, and Ph. Ebert, Appl. Phys. Lett. **82**, 2700 (2003).
[50]Ph. Ebert, T. Zhang, F. Kluge, M. Simon, Z. Zhang, and K. Urban, Phys. Rev. Lett. **83**, 757 (1999).
[51]S. Landrock, Y. Jiang, K. H. Wu, E. G. Wang, K. Urban, and Ph. Ebert, Appl. Phys. Lett. **95**, 072107 (2009).
[52]A. Samsavar, E. S. Hirschorn, T. Miller, F. M. Leibsle, J. A. Eades, and T.-C. Chiang, Phys. Rev. Lett. **65**, 1607 (1990).
[53]J. Wolf and H. Ibach, Appl. Phys. A **52**, 218 (1991).
[54]S. Vézian, J. Massies, F. Semond, N. Grandjean, and P. Vennéguès, Phys. Rev. B **61**, 7618 (2000).
[55]F. Nabarro, *Theory of Crystal Dislocations* (Clarendon Press, Oxford, 1967).
[56]A. Kelly and K. Knowles, *Crystallography and Crystal Defects*, 2nd ed. (Wiley, Cambridge, 2012), p. 255/256.
[57]D. Hull and D. J. Bacon, *Introduction to Dislocations*, 5th ed. (Elsevier, 2011).
[58]W. T. Read, *Dislocations in Crystals* (McGraw-Hill, New York, Toronto, London, 1953), pp. 116–117.
[59]G. I. Taylor, Proc. R. Soc. London, Ser. A **145**, 362 (1934).
[60]J. Burgers, Proc. K. Ned. Akad. Wet. **42**, 293 (1939).
[61]J. S. Koehler, Phys. Rev. **60**, 397 (1941).
[62]F. Nabarro, Adv. Phys. **1**, 269 (1952).
[63]P. Anongba, Phys. Status Solidi B **190**, 135 (1995).
[64]M. Schnedler, P. H. Weidlich, V. Portz, D. Weber, R. E. Dunin-Borkowski, and Ph. Ebert, Ultramicroscopy **136**, 86 (2014).
[65]E. Feltin, B. Beaumont, P. Vennéguès, M. Vaille, P. Gibart, T. Riemann, J. Christen, L. Dobos, and B. Pécz, J. Appl. Phys. **93**, 182 (2003).